Atmosphere carburizing using electric discharge-activated nitrogen-natural gas mixtures

Zbigniew Zurecki and Xiaolan Wang
Air Products& Chemicals, Inc., Allentown, Pennsylvania, USA
zureckz@airproducts.com and wangx222@airproducts.com

Abstract

Nitrogen-hydrocarbon gas atmospheres can offer a cost and part quality alternative to the conventional endothermic atmosphere and vacuum processes. Non-flammable, low percentage methane and nitrogen mixtures were activated during furnace injection by a novel, non-thermal electric discharge (cold plasma) method and used in carburizing process. Theoretical and experimental investigation has been carried out including box furnace tests at atmospheric pressure to examine the efficiency of activated mixtures in carburizing AISI 1010 shim stock and AISI 8620 steel parts between 875°C and 975°C. Laser gas analyzer was used to monitor changes in furnace CH_4, H_2, CO, CO_2, H_2O and residual O_2 concentrations during the process. Carbon mass flux (J, g/cm^2/sec), potential (C_p), activity (a_c) and carbon concentrations were evaluated. SEM-EDS examination has shown that, in addition to improving microhardness profile and increasing effective case depth, the new method eliminated internal oxidation defects identified in the comparable endo-carburized steel parts.

Introduction

Oxygen-free, hydrocarbon heat treating atmospheres have been an object of industrial and research interest for over quarter century. The early work of Kaspersma [1] and the subsequent studies [2-3] of 1-atm pressure, nitrogen-hydrocarbon blends (N_2-HC) have demonstrated that, due to a relatively high thermochemical stability, acceptable reaction rates can be obtained only by using more complex N_2-H_2-HC atmospheres, where the hydrocarbon is heavier than simple methane, and only at temperatures markedly higher than for the typical nitrocarburizing treatments. Similar observations were made in the area of vacuum carburizing where the initial practice of CH_4 carburizing at a fairly high partial pressure was gradually replaced by a low partial pressure carburizing in acetylene, ethylene, or propane-hydrogen multi-component blends [4-5]. This shift away from inexpensive CH_4 blends is not surprising in view of the recent HC dissociation data [6-7] as well the authors' own thermogravimetric measurements (TGA) illustrated in Fig. 1. The plots represent the carburization weight gain of AISI 1010 carbon steel coupons exposed to six different, non-flammable/non-explosive N_2-HC blends during a 10°C/minute temperature ramp-up. Results confirm that methane is practically nonreactive with steel up to 1000°C (1830°F). Acetylene starts an effective carburizing from about 700°C (1300°F), while propylene, propane (mixed with hydrogen or not), and ethylene become carburizing at the temperature 100°C-150°C higher. An important advantage of both the low-pressure and the 1-atm pressure hydrocarbon atmospheres over the conventional endothermic atmospheres is the absence of intergranual oxidation (IGO) of Mn, Si and, in the case of alloyed or microalloyed steels, also Cr, Al, Ti, or Zr [8-10]. Since IGO reduces fatigue strength, steel parts processed under endo-atmospheres require longer carburizing cycles, deeper carburized cases, and more stock to be ground-off during the subsequent machining. Marginally successful attempts to counter the endo-atmosphere resultant IGO by adding ammonia in the last minutes of carburizing [11] point to the value of oxygen-free hydrocarbon atmospheres in processing plain as well as low and highly alloyed steels.

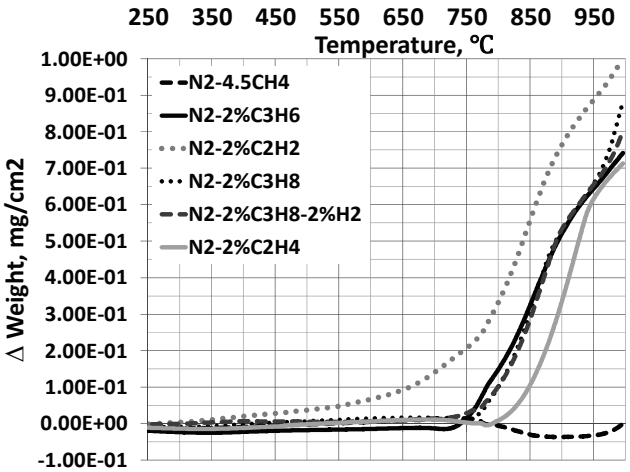

Fig. 1: TGA results of carburizing steel coupons in non-flammable (sub-LFL), thermally activated nitrogen-hydrocarbon gas blends at 1-atm pressure.

Against this background, the objective of present work is to explore the feasibility of carburizing steels in simple, non-toxic and non-flammable N_2-CH_4 atmospheres, with the CH_4

concentration kept below the low explosivity limit (LEL), which are activated at the inlet to heat treating furnace by a cold (non-thermal) plasma electric discharge.

Experimental

1. Cold Plasma Carburizing System

A series of gas stream-activating, cold-plasma injectors have been developed at Air Products during the recent few years. Described elsewhere [12], the injectors comprise two high voltage electrodes positioned across the stream of gas directed from gas supply into heat treating furnace. A DC or AC source-powered electric discharge between these electrodes ionizes, partially dissociates and converts the gas molecules on their way into the furnace. In contrast to the conventional, low-pressure plasma ion furnaces, metal load is not an electrode. A high-voltage/low-amperage, low power supply is used (typically below 2 kW) which forms a cold discharge combining self-pulsed, non-equilibrium arc and abnormal glow plasma modes [13] inside the passing gas stream. The low thermal energy of the discharge assures long electrode lifetime and prevents gas pyrolysis and sooting. Numerous long- and short-lived, equilibrium and non-equilibrium gas products are formed in the N_2-CH_4 blend passing the discharge.

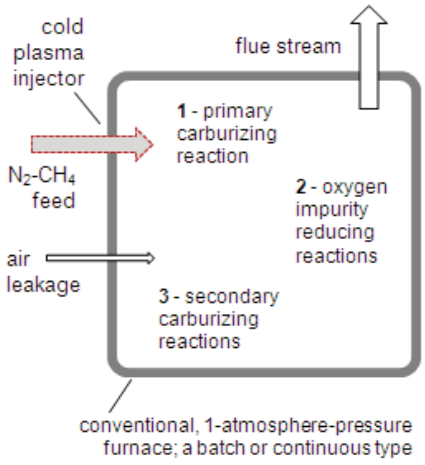

Fig. 2: Cold plasma activated gas injection system

They include ions, radicals, excited CH_4 and various byproducts: C_2H_2, C_3H_6, C_2H_4, CH_3, CH_2, C_3H_8, H_2, H, N, etc. [14-17], all readily reacting inside furnace and accelerating reducing and carburizing reactions at the surface of metal load. The plasma gas injectors can be easily retrofitted to various types of the conventional, radiant tube or electrically heated, 1-atm pressure and vacuum furnaces in order to carry out carburizing, carbonitriding, neutral carbon or "inert" annealing, as well as nitrocarburizing operations falling into a relatively low temperature range. Fig. 2 shows schematic of atmospheric, carburizing furnace equipped with the plasma gas injection retrofit.

Table 1: Reactions in atmospheric pressure furnace

Primary carburizing reaction: $m\ CH_4 \xrightarrow{plasma} C_mH_n + (2m - n/2)\ H_2$ $C_mH_n = m\ \underline{C} + n/2\ H_2$ $a_c = \{K\ p(C_mH_n)\ p(H_2)^{-2/n}\}^{1/m}$
Reduction of oxygen contamination in furnace volume: $O_2 + C_mH_n = CO + H_2O$ $O_2 + H_2 = H_2O$ $H_2O + C_mH_n = CO + H_2$ $CO + H_2O = CO_2 + H_2$ $CO_2 + C_mH_n = CO + H_2$
Secondary carburizing reaction – with contaminants: $CO + H_2 = C + H_2O$ $a_c = K\ p(CO)\ p(H_2) / p(H_2O)$
where: C_mH_n - plasma activated hydrocarbon, p – gas partial pressure, a_c – activity of carbon in gas phase, and K = K(T) – reaction equilibrium constant

The primary carburizing reaction involves plasma activated hydrocarbon molecules, C_mH_n, and metal surface. Additional, oxygen reducing reactions may also take place in the case of air infiltration of the furnace or air leakage which results in formation of trace quantities of gases contained in the conventional endo-atmospheres. These products may, in turn, lead to secondary carburizing reactions listed in Table 1. Cold plasma carburizing process can be controlled using a modified version of the conventional (thermal), low-pressure (vacuum) and atmospheric pressure modeling approaches developed by the Center for Heat Treating Excellence at Worcester Polytechnic Institute [18] and represented in Fig. 3.

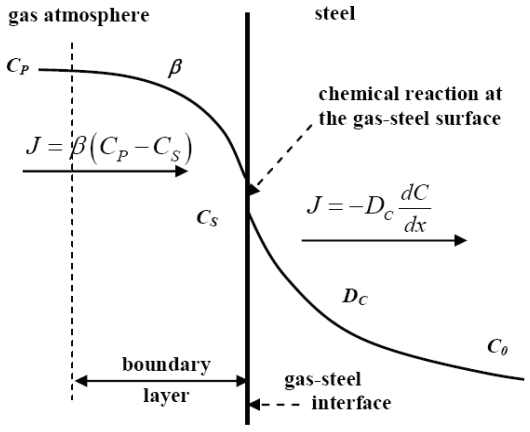

Fig. 3: Carbon transport in gas carburizing

Expressions (1-5) combine the main control factors for the N_2-CH_4 plasma carburization: total gas feed rate through plasma injector, CH_4 concentration in the feed stream, plasma power applied, process time and temperature, as well as furnace flow field and furnace heaters characteristics. Optional gas analysis

of the flue stream could be used for monitoring H_2, H_2O, CO, CO_2, and/or residual CH_4 to detect operational or furnace problems.

(1) $J = \beta (C_p^* - C_s)$

(2) $C_p^* = C_p \{p(C_mH_n)\}$

(3) $p(C_mH_n) = f \{C_{CH4}, E_{activ}, T_f, T_h\}$

(4) $E_{activ} = P_{plasma}/Q_{N2\text{-}CH4}$

(5) $J_t = \Delta m/A/t$

where: J - carbon mass flux in activated hydrocarbon atmosphere, g/cm^2/sec, $\beta = \beta(F)$ - mass transfer coefficient, a function of gas properties and flow field F, cm/sec, C_p^* - apparent carbon potential of activated hydrocarbon atmosphere, a function of activated hydrocarbon partial pressure, wt%, g/cm^3, $C_s = C_s(T_f, t)$ - carbon content at steel surface, a function of furnace temperature, T_f, and time, t, wt%, g/cm^3, $p(C_mH_n)$ - partial pressure of activated hydrocarbon gases, a function of CH_4 concentration in the feed stream, C_{CH4}, plasma energy absorbed by the N_2-CH_4 feed stream, E_{activ}, furnace temperature, T_f, and furnace heaters temperature, T_h, $P_{plasma}/Q_{N2\text{-}CH4}$ - plasma discharge power per mass flowrate of the N_2-CH_4 feed stream, J/g, and J_t - time averaged carbon flux measured by weight gain, Δm, per exposure interval, t, of shim stock having surface area A, g/cm^2/sec.

2. Procedures

Atmosphere carburizing experiments were run in a semi-production scale, electrically heated box furnace, ATS 3350, configured as in Fig. 2. The inlet concentration of CH_4 in N_2-stream was always kept below LEL (<5 vol %), and no air was intentionally added to the furnace. In the first part of test program, shim stock coupons were exposed to carburizing atmospheres to assess carbon flux, apparent carbon potential, and carbon activity in gas phase. In the second part of tests, real production parts were carburized, quenched in oil, and tempered in order to compare the plasma activated carburizing to the conventional, endothermic atmosphere carburizing.

Three different thickness levels of AISI 1010 steel shim stock, 4 x4 in^2 (103.2 cm^2) were used: 0.004-inch (102 μm), 0.015-inch (381 μm), and 0.031-inch (787 μm). Carburization of these specimens was performed according to the conditions given in Table 2. Test 1 was performed under non-activated gas atmosphere; the others used AC-plasma activation. Each carburization cycle involved ¾-hour long heating of acetone-degreased specimens from room to treatment temperature under pure N_2, 3-hour carburizing and 3-hour cooling with furnace to room temperature under pure N_2. The specimens were weighted before and after the carburizing cycle. Weight gain, Δm, and final weight, m_f, were used to determine the apparent atmosphere carbon potential, C_p^*, according to equations 5 and 6, where C_o, the initial carbon was < 0.1 wt%.

(6) $C_p^* = 100\, J_t\, A\, t / m_f + C_o = 100\, \Delta m / m_f + C_o$

Production parts were investment cast and machined AISI 8620 steel rings (R), 44 mm dia, and shafts (S), 14 mm dia. Table 3 presents nominal composition of the steel used.

Table 2: Shim stock carburizing conditions

Test No.	T1	T2	T3	T4
Temperature (℃)	875	875	975	975
Carburizing Time(hr)	3	3	3	3
Plasma activation	None	Yes	Yes	Yes
Gas Flowrates, scfh (Nm^3/h at 0^{o}C)				
Total gas flowrate	250 (6.7)	250 (6.7)	250 (6.7)	500 (13.4)
N_2-thru-plasma	0	239 (6.4)	239 (6.4)	478 (12.8)
CH_4-thru-plasma	0	11 (0.29)	11 (0.29)	22 (0.58)
Furnace inlet CH_4 (vol %)	4.5	4.5	4.5	4.5

Three pairs of R and S parts were tested: the 1st was endo-atmosphere carburized at a commercial heat treating shop using an integral quench furnace and ZrO_2-probe control, the 2nd was carburized using DC-plasma activation, and the 3rd was carburized using AC-plasma activation, both in the ATS box furnace. The endo-atmosphere treatment was executed as follows: the parts were loaded to hot furnace at 900^{o}C with the carbon potential, Cp, maintained at 0.95 wt%C and boost-carburized for 2.5 hours, then, diffused at Cp of 0.8-0.9 wt%C for 0.5 hours at the temperature reduced to 843^{o}C, quenched in oil tank inside the furnace and, finally, low-tempered at 180^{o}C for 2 hours. The DC and AC plasma-activated carburizing treatments were executed in a somewhat simplified way: the parts were loaded to hot furnace filled only with a technically pure N_2 (99.995%) at 900^{o}C, the CH_4 flow and plasma power were turned on after part loading. Only one total gas flowrate of 300 scfh and CH_4 inlet concentration of 4.6vol% was used during the subsequent 2.5-hr boosting at 900^{o}C and 0.5-hr diffusing at 843^{o}C. The parts were manually transferred through ambient air into an external oil bath at the end of diffusing step. The last, 2-hr tempering step at 180^{o}C was carried out under a plasma-activated, N_2-2.2 vol%CH_4 stream.

Table 3: AISI 8620 steel composition (wt. %)

C	Mn	P	S	Si	Ni	Cr	Mo
0.18-0.23	0.7-0.9	<0.03	<0.04	0.15-0.35	0.4-0.7	0.4-0.6	0.15-0.25

Laser gas analyzer (LGA), manufactured by ARI, model LGA-4ENAPBT, was used to measure the inlet and the flue gas concentrations throughout the entire testing program. H_2, CH_4, CO, CO_2, O_2, N_2 and H_2O concentrations were tracked with accuracy of <50 ppm. Superficial hardness HR15N on the outer diameters, and Vickers microhardness profiles, 300 g load @ 10 sec, were taken for the fully carburized, quenched,

and tempered R and S parts. Metallographic cross-sections of the parts were etched with 2% Nital prior to SEM-EDS examination.

Result and discussion

Apparent carbon potential of N_2-CH_4 atmospheres calculated from eq. 6 for the fixed carburizing time of 3 hours was higher than typical carbon potentials expected in the conventional endothermic atmospheres, Table 4. This is not surprising in view of literature references on O_2-free, HC atmospheres [1-2 and 19] where the equilibrium products of HC carburizing are cementite (6.67 wt%C) or soot. Interestingly, the apparent carbon potential differed for the thinner (102 µm) and thicker (381 µm) shim coupons due to the fact that the thinner shim saturated with carbon much faster.

Table 4: Carbon potential and carbon activity in gas phase

.

Test No.	T1	T2	T3	T4
Apparent carbon potential, C_p^*, wt%C, calculated from weight gain measurements				
0.004"	2.04 ±0.05	2.74 ±0.08	3.40 ±0.07	2.44 ±0.11
0.015"	0.89±0.04	1.63 ±0.05	1.79 ±0.02	1.75 ±0.03
Carbon activity in gas phase, a_c ,calculated from H_2 and CH_4 concentrations in furnace				
a_c	1.9E+05	4.6E+04	1.8E+04	7.2E+04

Additional diffusion modeling work was performed using the *CarbTool* software referenced in [18] which confirmed the saturation effect rather than the presence of a carbon gradient in the thicker shim coupons. Carbon activity in gas phase was calculated per procedure described in [19] using averaged LGA measurements of H_2 and CH_4 concentrations in the furnace flue stream for the gas carburizing reaction of CH_4 = C + $2H_2$ which ignores plasma activation effects. *Chemical Reaction and Equilibrium Software*, Outokumpu HSC Chemistry® for Windows with JANAF database, version 5.1 02103-ORC-T, was used for the activity calculations.

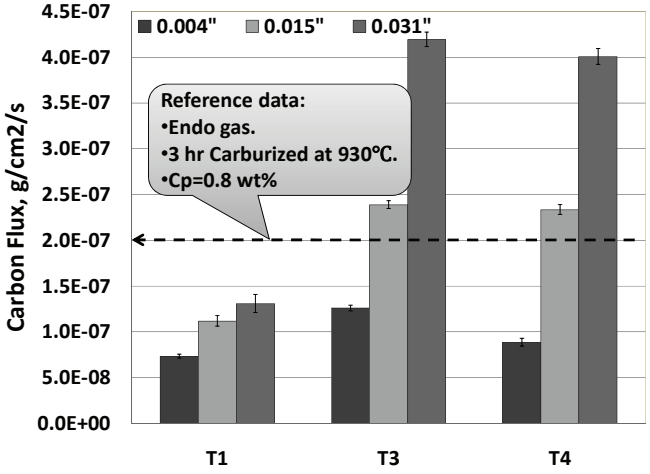

Fig. 4: Effect of shim stock thickness on carbon flux measurement (3hr carburizing, N_2- 4.5 vol% CH_4)

The results shown in Table 4 clearly indicate that the activity was orders of magnitude higher than in the case of conventional endothermic atmospheres but, also, deviated from the carbon potential. Thus, a_c was the highest for a marginally carburizing T1 condition and the lowest for the most carburizing, plasma-activated condition T3. This spread between the weight gain based C_p^* values and the atmosphere composition based a_c values is the direct evidence of the plasma activation effect. Appendix 1 details experimental errors.

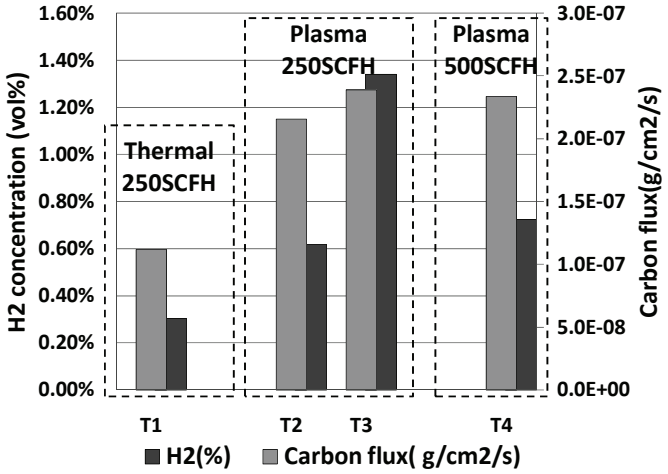

Fig. 5: Thermal and plasma carburizing using N_2-4.5 vol% CH_4 gas blend (AISI 1010 steel, 0.015" shim stock)

Just like in the case of low-pressure (vacuum) carburizing and, to a large degree in endo-atmosphere carburizing, carbon mass flux is, perhaps, the most practical measure of the plasma-activated carburizing process that enables the operator to compare various process conditions and predict outcomes.

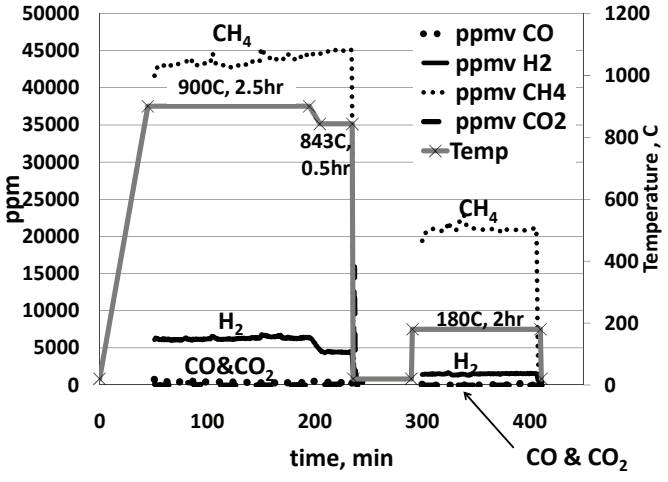

Fig. 6: LGA plot of flue gas composition during AC plasma carburizing and tempering of R and S parts

Fig. 4 and 5 show the effect of shim stock thickness, process temperature, and N_2-4.5 vol%CH_4 gas blend flowrate at fixed plasma power input on carbon flux, J_t, averaged over a 3-hour exposure. Thus, the plasma activated conditions T3 and T4

produced at least as high flux values as the endo-atmosphere carburizing evaluated in [20] or vacuum furnace carburizing with propane [21]. On the other hand, the non-activated, purely thermal condition T1 resulted in an unacceptably low carbon flux, even though its a_c and C_p^* values were high. In the plasma activated runs T2-T4, carbon flux scales much more with the plasma energy absorbed by the incoming gas, E_{activ}, eq. 4, and furnace temperature, than with the degree of CH_4 dissociation indicated by the level of H_2 in atmosphere shown in Fig. 5. It is concluded that the formation of active C_mH_n groups plays a critical role in cold plasma carburizing. Fig. 6 illustrates the typical carburizing, oil quenching, and tempering treatment cycle of the production parts R and S processed with the AC and DC cold plasma system. For the boosting and diffusing steps, the flue stream analysis was as follows: CH_4 ≤4.4 vol%, H_2<1.0 vol%, CO_2<0.1 vol%, CO<0.05 vol%, H_2O< 50 ppm (dew point below -48°C or -54°F) and O_2 below the LGA detection limit of 50 ppm. Oxygen adsorbed on furnace refractories, oxide films, and a minute air leakage were the most likely sources of oxygen detected in the effluent. The trace level of the gases required for the secondary, 'endo-like' carburizing reaction provided no support for the conventional a_c and C_p calculations proposed first by Collin *et al*. [22] and indicated that only the primary reaction, $C_mH_n = m\,\underline{C} + n/2\,H_2$, was operational. For the tempering step, where the inlet CH_4 level was reduced, the concentrations of the flue components were correspondingly lower. Of note, the conversion of the CH_4 injected and the H_2 production scaled with the furnace temperature throughout the treatment cycle.

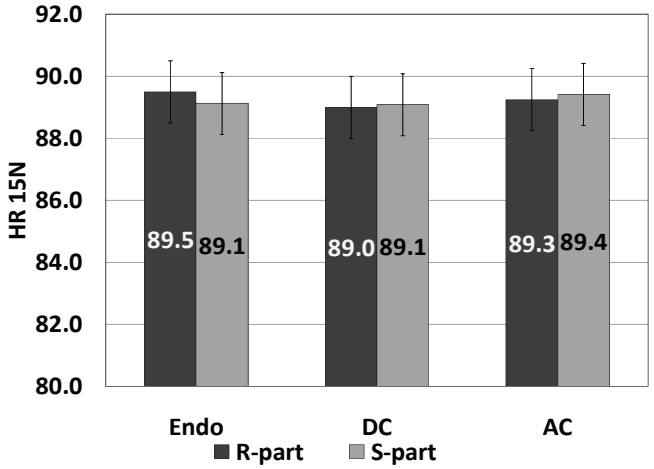

Fig. 7: Hardness HR15N of endo-atmosphere and plasma (DC and AC) carburized, oil quenched, and tempered ring (R) and shaft (S) parts

Superficial hardness measurement is a convenient method of spot-checking part quality in a stabilized carburizing heat treatment processes. The superficial hardness HR15N of the endo-atmosphere, DC-plasma, and AC-plasma carburized and heat treated parts R and S was measured and found to be identical within a narrow range of measurement error, Fig.7. A far more complete picture of a carburizing heat treatment process is obtained by a microhardness profiling as shown in Fig. 8 and 9.

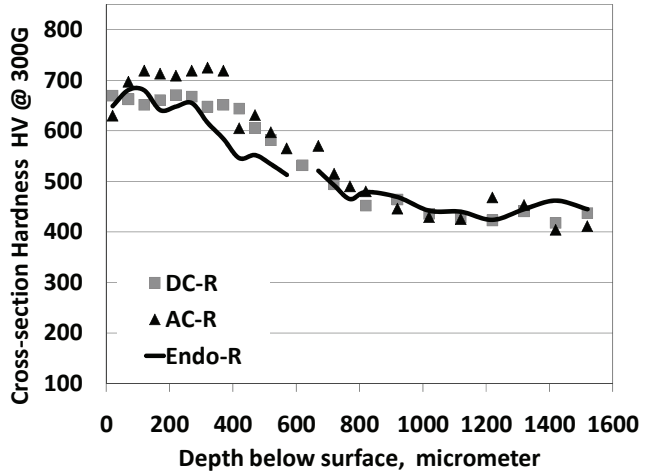

Fig. 8: Vickers microhardness profile for endo-atmosphere and plasma (DC and AC) carburized, oil quenched, and tempered ring (R) parts

Although the surface hardness of all samples was nearly identical, the cross-section hardness profile exhibited differences. The DC and AC plasma samples displayed a higher hardness level (higher carbon content and/or lower retained austenite) going deeper into the part with a sharper drop-off in the core area than the endo samples. This type of hardness profile is valuable, especially, in the case of parts requiring an additional finish-machining of the surface for restoring dimensional accuracy. Evaluated as in [23], the effective case depth (ECD) for 50 HRC in the plasma carburized parts was 0.700 mm (0.0276 inches), i.e. somewhat larger than in the endo-atmosphere carburized parts. Analyses of the furnace atmosphere gases as well as the steel carburizing data have shown that the DC and the AC powered electric discharges are comparable from the effectiveness standpoint.

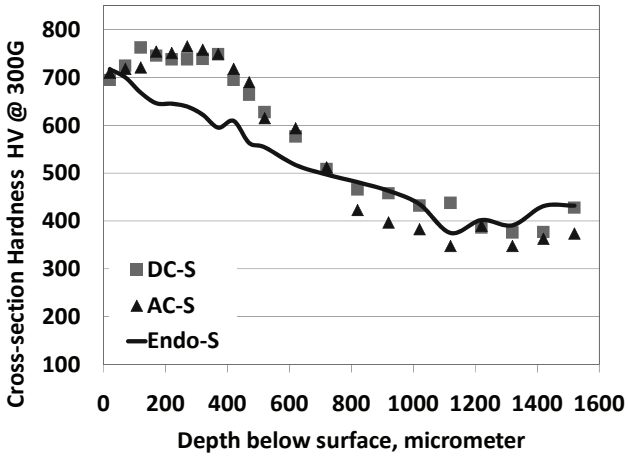

Fig. 9: *Vickers microhardness profile for endo-atmosphere and plasma (DC and AC) carburized, oil quenched, and tempered shaft (S) parts*

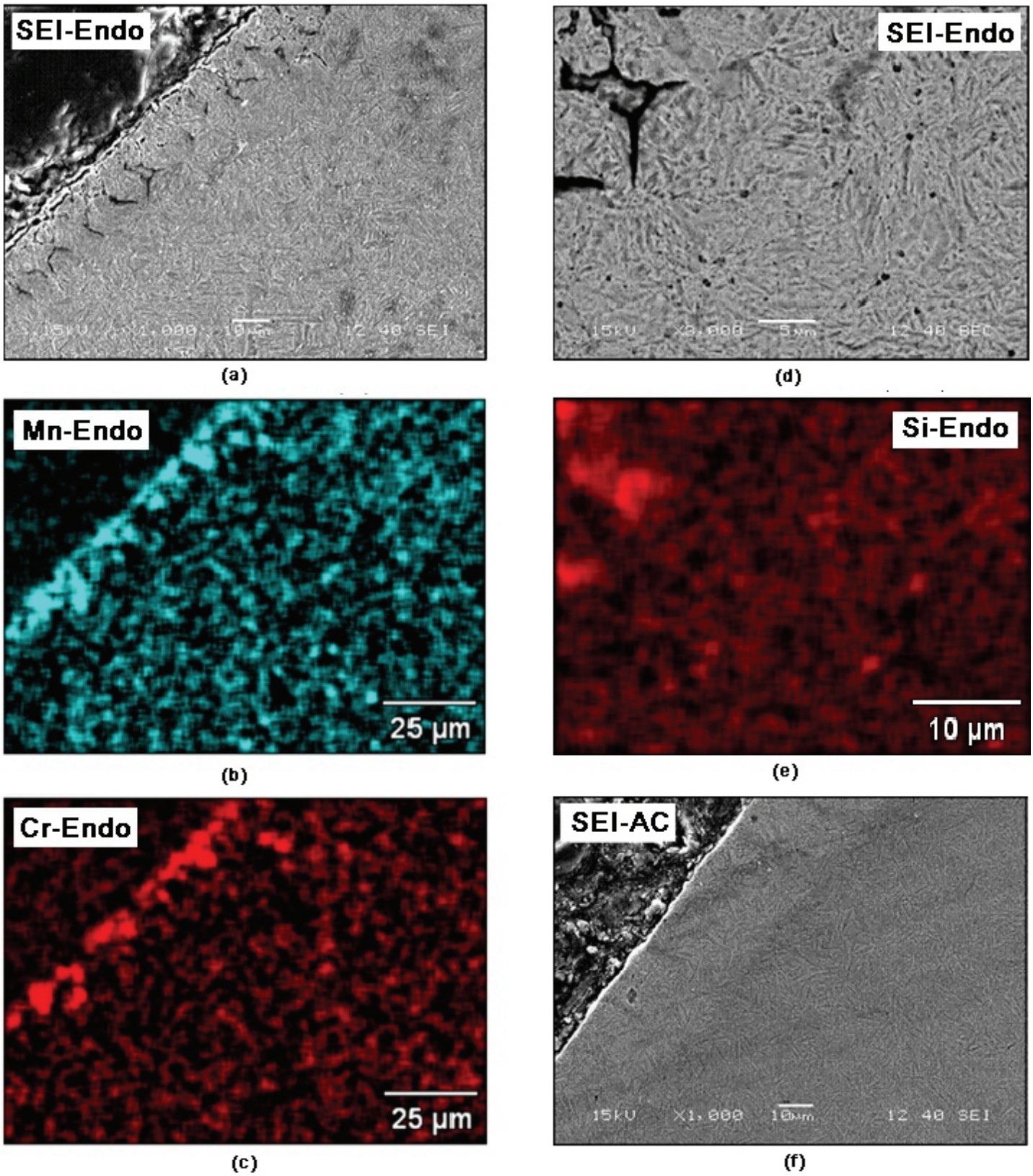

Fig. 10: SEM-SEI-EDS cross-sectional images of subsurface regions of production parts S after completed carburizing, quenching and tempering cycle. Etched in 2% Nital. (a) SEI image of endo-atmosphere carburized part; (b-c) Mn and Cr EDS-maps of area (a), (d) higher magnification of area (a), (e) Si EDS-map of area (d); and (f) SEI image of AC-plasma carburized part.

Cross-sectional secondary electron images (SEI) of the endo-atmosphere and plasma carburized parts S, and the corresponding, elemental maps of Mn, Cr and Si were acquired using SEM energy-dispersive X-ray spectroscopy (EDS) probe, Fig. 10. The endo-carburized part revealed a clearly developed intergranular oxidation zone with the depth that agrees with the diffusional calculations and experimental data presented in [8]. The enrichment of the oxidized boundaries with Mn, Cr and Si was observed and explained by a higher affinity of those Fe-alloying elements for oxygen and oxygen-containing gases always present in all types of endothermic carburizing atmospheres [11]. In contrast, no IGO effect was observed in the AC and DC plasma carburized samples that exhibited a vacuum carburizing quality of surface and subsurface material.

Conclusions

1. Cold, non-equilibrium plasma system has been explored and successfully demonstrated in carburizing steels at 1-atm pressure using CH_4-lean, non-flammable/non-explosive N_2-CH_4 atmospheres. Easy to install in the conventional furnaces, the cold plasma system minimizes environmental pollution and offers a nearly 100%, instant turndown ratio. The DC and the AC electric discharges were found to be comparably effective in the activation of gas stream during injection and carburizing of metal surface.
2. Steel carburizing reactions and process kinetics were evaluated. The surface reaction with excited hydrocarbons produced during the passage of CH_4 through plasma discharge appears to dominate the process. Measurements of carbon mass flux and calculations of carbon potential and activity in gas phase have shown that the present carburizing rates are comparable to those of low-pressure (vacuum) and endothermic atmosphere carburizing systems, but the thermodynamic equilibrium cannot be established. Nevertheless, process control is simple, mass flux based, and the popular, low-pressure carburizing models are applicable.
3. Carburizing effects were compared for the AISI 8620 steel rings and shafts processed with the plasma-activated N_2-4.5 vol%CH_4 mixture and the conventional endothermic atmosphere using the same heat treatment schedule. The plasma atmosphere processed parts were completely IGO-free and revealed a somewhat deeper effective carburized depth. The microhardness profile directly under metal surface was relatively flat, reminding the profiles obtained by low-pressure carburizing, and beneficial from the post-machining and fatigue strength standpoint. In contrast, the endo-atmosphere carburizing resulted in IGO defects, with the associated Mn, Cr and Si grain boundary enrichment, and a steep slope of the hardness profile.
4. The further work will include predictive process control using diffusional modeling of carbon profile and fluid dynamics in large-size, continuous and pit-type furnaces.

Acknowledgments

The authors would like to thank Messrs. J. Conybear and D.J. Bowe for valuable industrial suggestions, Dr. S.P. Gangoli for plasma technology contributions, Messrs. J.R. Stets, R.E. Knorr, J.L. Green for laboratory support, Prof. R.D. Sisson for access to *CarbTool* software, and Air Products' management for the permission to publish this study. Article first presented at 2010 ASM Heat Treating Society Conference. Reprinted with permission of ASM International.

References

[1] Kaspersma, J.H., and Shay, R.H., "Carburization and Gas Reactions of Hydrocarbon-Nitrogen Mixtures at 850°C and 925°C", *Metallurgical Transactions B*, Vol. 13B, June 1982, pp. 267-273.

[2] Estrin, B.M, *et al*, "Carburizing in a nitrogen-based mixture with additives of pure methane", *Metallovedenie i Termicheskaya Obrabotka Metallov*, No. 5, pp. 26-29, May, 1984

[3] Connery, K. and Ho, S., "Optimization of Oxygen-free Heat Treating", *Proc. of the 24th ASM Heat Treating Society Conf.*, September 17-19, 2007, COBO Center, Detroit, Michigan, USA

[4] Tsuji, S., *et al*, "Vacuum Carburizing of Low Carbon Steel with Methane", *Trans. of the Japan Institute of Metals*, Vol. 28, No.1 (1987), pp. 48-56

[5] Gorockiewicz , R., *et al*, "The Benefits of Using 3 Gas Mixture Low Pressure Carburizing (LPC) for High Alloy Steels", *Proc. of the 24th ASM Heat Treating Society Conf.*, September 17-19, 2007, COBO Center, Detroit, Michigan, USA

[6] Shah, N., *et al*, "Hydrogen Production by Catalytic Decomposition of Methane", *Energy & Fuels*, 2001, *15,* 1528-1534

[7] Khan, R.U., *et al*, "Pyrolysis of propane under vacuum carburizing conditions: An experimental and modeling study", *J. Anal. Appl. Pyrolysis* 81 (2008) 148–156

[8] Chatterjee-Fisher, R., "Internal Oxidation During Carburizing and Heat Treating", *Metallurgical Transactions* Vol. 9A, November 1978, pp.1553-1560

[9] An, X., *et al*, "A study of internal oxidation in carburized steels by glow discharge optical emission spectroscopy and scanning electron microscopy", *Spectrochimica Acta Part B* 58 (2003), pp. 689–698

[10] Asi, O., *et al*, "The relationship between case depth and bending fatigue strength of gas carburized SAE 8620 steel", *Surface & Coatings Technology* 201 (2007), pp. 5979–5987

[11] Kozlovskii, I.S., et al, "Internal oxidation during case-hardening of steels in endothermic atmospheres", *Metallovedenie i Termicheskaya Obrabotka Metallov*, No. 3, pp. 2-7, March 1967

[12] Zurecki, Z., "Heat Treating Atmosphere Activation", , *Proc. of the 24th ASM Heat Treating Society Conf.*, September 17-19, 2007, COBO Center, Detroit, Michigan, USA

[13] Fridman, A., Plasma Chemistry, Cambridge University Press (New York, 2008), pp. 177-208
[14] Li, Xiao-Song, *et al*., "Methane conversion to C2 hydrocarbons and hydrogen in atmospheric non-thermal plasmas generated by different electric discharge techniques", *Catalysis Today* 98 (2004) 617–624
[15] Zhaoa, G-B., et al., "Methane conversion in pulsed corona discharge reactors", *Chemical Engineering Journal* 125 (2006) 67–79
[16] Kado, S., *et al*., "Diagnosis of atmospheric pressure low temperature plasma and application to high efficient methane conversion", *Catalysis Today* 89 (2004) 47–55
[17] Indarto, A., *et al*., "Effect of additive gases on methane conversion using gliding arc discharge", *Energy* 31 (2006) 2986–2995
[18] Karabelchtchikova, O., *et al*., "New Carburizing Calculation Tool for Gas and Low-Pressure Carburizing, A CHTE Project Summary", *Heat Treating Progress*, March/April 2008, p. 18
[19] Forseth, S., and Kofstad, P., "Carburization of Fe-Ni-Cr steels in CH_4-H_2 mixtures at 850±1000°C", *Materials and Corrosion* 49, 266±271 (1998)
[20] Linde Gas, Special Edition, "Furnace Atmospheres No. 1, Gas Carburizing and Carbonitriding", url: https://b2.boc.com/catweb/CATweb.nsf/noteid/EC84EBA1ADCB86EC802572C1004B3977/$file/SpEd_Carburizing_and_Carbonitriding.pdf, last accessed: March 24, 2009
[21] Altena, H., and Schrank, F., "Low Pressure Carburizing with High Pressure Gas Quenching", *Gear Technology*, March/April 2004, pp.27-32
[22] R. Collin, R., *et al*, "Mathematical Model for Predicting Carbon Concentration Profiles of Gas-Carburized Steel," *Journal of the Iron and Steel Institute*, 210 (1972), 785-789
[23] Thomas, J., *et al*, "High Production Gas Carburizing of Transmission Gears and Shafts", *The 21st ASM Heat Treating Society Conference Proceedings*, 5-8 November 2001, Indianapolis, IN, ASM International

Appendix 1

Estimation of measurement errors in calculation of apparent carbon potential, C_p^*, and average carbon flux, J_t, displayed in Table 4 and Figure 4:

[**A**] Error of C_p^* calculated using equation (6) is affected by measurement of Δm, i.e. the difference between m_f and m_o, and C_o. The C_p^* error is estimated using partial derivative method:

$$\Delta C_p^* = \sqrt{\left(\frac{\partial Cp}{\partial m_f}\right)^2 \Delta m_f{}^2 + \left(\frac{\partial Cp}{\partial m_o}\right)^2 \Delta m_o{}^2 + \left(\frac{\partial Cp}{\partial C_o}\right)^2 \Delta C_o{}^2}$$

$$\Delta C_p^* = \sqrt{\left(\frac{100 m_o}{m_f{}^2}\right)^2 \Delta m_f{}^2 + \left(-\frac{100}{m_f}\right)^2 \Delta m_o{}^2 + \Delta Co^2}$$

[**B**] J_t error is affected by measurement of m_o, m_f, and time, t; our rolled shim stock thickness, w, was considered consistent.

$$J_t = \frac{\frac{(m_f - m_o)}{A}}{t} = \frac{w\rho}{2t} \cdot \frac{(m_f - m_o)}{m_o}$$

$$\Delta J_t = \sqrt{\left(\frac{\partial J_t}{\partial m_f}\right)^2 \Delta m_f{}^2 + \left(\frac{\partial J_t}{\partial m_o}\right)^2 \Delta m_o{}^2 + \left(\frac{\partial J_t}{\partial t}\right)^2 \Delta t^2} =$$

$$= \frac{w\rho}{2} \sqrt{\left(\frac{1}{m_o t}\right)^2 \Delta m_f{}^2 + \left(-\frac{m_f}{m_o{}^2 t}\right)^2 \Delta m_o{}^2 + \left(\frac{m_o - m_f}{m_o t^2}\right)^2 \Delta t^2}$$

where:

- m_f – final weight of shim coupons (after carburizing),
- m_o – initial weight of shim coupons, and $\Delta m = m_f - m_o$,
- t – carburizing (exposure) time, t = 3 hrs, Δt = 120sec,
- w – thickness of shim stock used: 0.004-inch (0.10 mm), 0.015-inch (0.38 mm), and 0.031-inch (0.79 mm),
- C_o – initial carbon content of shim coupons, C_o = 0.084 %wt C and 0.081%wt C, based on Leco extractive analysis of AISI 1010 used, ΔC_o = 0.003 wt% C, and
- A - effective carburizing surface, calculated from initial coupon weight and density, ρ.

[**C**] C_p^* values were also compared to the carbon content predicted by a β-version of the *CarbTool* software [18] using our shim-measured carbon flux, J_t, and the vacuum furnace carburizing model. The predicted values diverged from the measured ones within a ±10% range which indicates that, with the carbon flux data available, vacuum carburizing models can be used to predict outcome of cold plasma carburizing. Measured values of flux J_t were used to model carbon profile in the AISI 8620 part S during the AC-plasma carburizing, Fig. 11. While no chemical analysis of carbon case was done in this study, the predicted carbon profile appears to follow the microhardness profile shown in Fig. 9, quite well except for the first 50 µm of this quenched and tempered material.

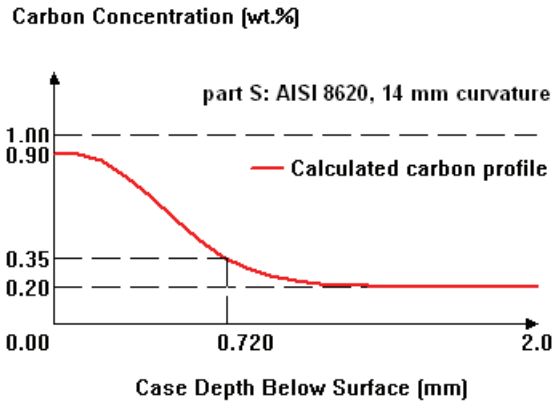

Fig. 11: CarbTool prediction of carbon profile for the AC-plasma carburizing of the AISI 8620 parts S.